EASR

Engineering and Applied Science Research

https://www.tci-thaijo.org/index.php/easr/index

Published by the Faculty of Engineering, Khon Kaen University, Thailand

Effect of warm deformation parameters on hardness and microstructure of AISI 1020 low carbon steel for near-net shape forging

Napatsakorn Jhonthong and Sukangkana Talangkun*

Department of Industrial Engineering, Faculty of Engineering, Khon Kaen University, Khon Kaen 40000, Thailand

Received 12 December 2024
Revised 28 January 2025
Accepted 17 February 2025

Abstract

This research aims to present a concept for altering a metal manufacturing process from cold to warm forging thereby reducing unnecessary steps and energy consumption. This will lower costs and increase production profits. The study explores the impact of warm forging process parameters on the hardness and microstructure of low-carbon steel for near-net-shape forging in more than two continuous stages. The material used in this experiment is annealed AISI 1020 carbon steel with chemical additions of 0.01% Ni, 0.03% Cr, and 0.044% Al. The study procedure involves: (i) heating slugs with a height-to-diameter ratio (ho/do) of 2.07 to a temperature range of 200–700 ℃ and soaking them for 1 hour. The grain size noticeably increases at temperatures above 500 °C. (ii) The materials were forged at six different temperatures from 200 to 700 ℃ with both hardness and microstructure examined at each stage. This was done to determine the recrystallization temperature. The experimental results showed that recrystallization begins at 500 ℃ in a warm forging process and becomes more pronounced at 600 to 700 °C. The lowest average hardness value in the transverse direction (TD) occurs at 500 to 700 °C. This suggests that the suitable warm working temperature range should be below 500 °C, as the primary microstructure in the forging process has not yet undergone recrystallization. Our research provides valuable insights for manufacturers aiming to transition from cold to warm forging, emphasizing the importance of precise control over deformation parameters to achieve desired material properties.

Keywords: Warm forging, Warm deformation, Upsetting, Low carbon steel

1. Introduction

In a metal-forming process, one of the crucial factors is the forging temperature. It has significant impacts on the mechanical properties and energy used in forging. Forging temperatures are divided into three categories. They are cold forging, which involves forging at room temperature; warm forging, which occurs at a temperature higher than room temperature but below the material's recrystallization temperature, and hot forging, which is conducted at a temperature above the recrystallization temperature but below the melting point of the material [1-4]. In recent years, researchers have studied various parameters affecting material behavior in warm forging processes, especially the impact of composition on the behavior of low-carbon steels with no more than 0.2% C. Low-carbon steel remains a popular material for forging parts in various industries, including automotive, machinery, electrical equipment, and other components [4-6]. Forging parameters can have a significant impact on the mechanical properties and microstructure of AISI 1020 low-carbon steel [2, 6]. Understanding these parameters is crucial for optimizing material properties. For example, the temperature range during warm forging is important because it affects the flow stress, ductility, and recrystallization behavior of a material [7-9]. Higher temperatures often increase ductility and reduce flow stress, making deformation easier. However, precise temperature control is necessary to avoid excessive grain growth or phase transformation [10-12]. Important forging factors include the (i) strain rate, which affects the microstructure by influencing grain size, dislocation density, and texture formation. It also impacts recrystallization by altering activation energies, nucleation sites, and grain growth dynamics. These factors are crucial in optimizing material properties and performance in metal-forming processes [13-15]. (ii) Deformation degree is the extent of deformation applied to a material which affects grain sizes and the distribution of dislocations. Higher deformations typically result in finer grains and a more uniform microstructure [16-19]. (iii) Holding time is the length of time that a material remains at the forging temperature. It can impact both grain growth and phase stability. Longer holding times may lead to grain coarsening, while shorter times can preserve fine-grain structures [6, 20, 21]. The rate at which the material cools after forging impacts phase transformations and the final microstructure. Rapid cooling (quenching) can result in a martensitic structure in steels, while slow cooling can lead to ferrite or pearlite structures [16, 22-24]. (iv) The initial microstructure of the material before forging plays a role in determining its final microstructure. Pre-forging treatments, such as annealing, normalizing, or prior deformation history, can influence how a material responds to warm forging. In addition to the aforementioned forming factors, particularly in cold and hot forging processes, there are various other influencing factors. These include high force requirements, limited material flow, challenges in forming complex shapes, surface defects such as cracking, and work hardening. Such factors can complicate subsequent processing steps and necessitate annealing in cold forging. Scale can form on the surface of a workpiece during hot forging, which can lower the quality of the surface and require extra cleaning

*Corresponding author.
Email address: sukangkana@kku.ac.th
doi: 10.14456/easr.2025.16

steps. High temperatures can also cause dimensional errors and change a material's microstructure and mechanical properties. Warm working widens the range of applicable steel grades that can be forged and allows forming of higher alloyed steels. Therefore, the main advantage of this method is to attain practically the same tolerances as cold forging and to achieve the same formability as hot forging [1-4]. For example, cold forging of an automotive part currently involves a three step forging process. The initial material normally has undergone hot rolling and annealing. Then, it is (i) cut into slugs, (ii) subjected to upset forging followed by annealing at 800–900 ℃ for 6-8 hours, cleaning with shot blast and soap phosphate coating lubricant before entering the cold forging process. (iii) Cold forging Step 1 involves backward extrusion to shape the workpiece into a cup-like form. After this process, the workpiece is cleaned with shot blast and coated with soap phosphate lubricant. (iv) Cold forging Step 2 is when gear teeth are formed at the rim of the workpiece. The workpiece then undergoes drilling and final surface finishing using a lathe. The current process involves many production steps and the workpiece has high residual stresses after cold forging, necessitating at least 24 hours to improve the mechanical properties of the workpiece to enable further forging steps.

This research aims to explore alternative production processes to mitigate these drawbacks. Specifically, the study focuses on using a warm forging process to identify the most suitable parameters for forming AISI 1020 low-carbon steel. The specified material has a chemical composition (mass fraction) of 1% Ni, 2% Cr, and 3% Al added to the standard AISI 1020. This material is commonly used to manufacture industrial components in the automotive, machinery, and equipment sectors. By conducting a warm forging process at temperatures below the Ac_1 line in the phase diagram, the research seeks to determine the optimal temperature and the effects of warm deformation parameters on the hardness and microstructure of the material to achieve a near-net shape of the final workpiece.

2. Experimental setup and procedures/methods

2.1 Material testing

The chemical composition of annealed AISI 1020 mild carbon steel specimens compared with the standard is detailed in Table 1. The specimen preparation process involves cutting the material from a hot rolled coil into a 20+0/-0.05 mm section and using a cut-off die to form pieces with lengths of 41.40±0.05 mm, as illustrated in Figure 1.

Table 1 Chemical composition of AISI 1020 steel (mass %)

	C	Si	Mn	P	S	Ni	Cr	Al	Fe
AISI 1020 Standard	0.18~0.23	0.15~0.35	0.30~0.60	0.03 max	0.035 max	-	-	-	Balance
as received	0.2	0.2	0.007	0.02	0.45	0.01	0.03	0.044	Balance

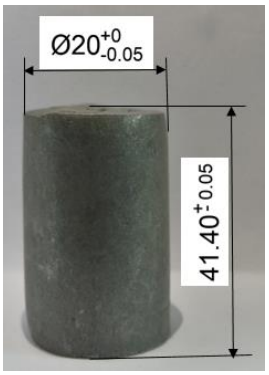

Figure 1 Example of the initial slug cut by shearing. Scale in mm.

2.2 Heat treatment

The specimens were drilled in the center forming a 0.6 cm diameter hole to a 1.5 cm depth enabling attachment of Type K thermocouples for temperature measurement of the test piece, as shown in Figure 2. The specimens were placed inside a Linn High Therm KS80 high-temperature furnace. They were heated to different temperatures, including 200, 300, 400, 500, 600, and 700 ℃, at a rate of 10 ℃/min. Then, they were held at these temperatures for 1 hour [25]. Subsequently, specimens were quenched with water as shown schematically in Figure 3.

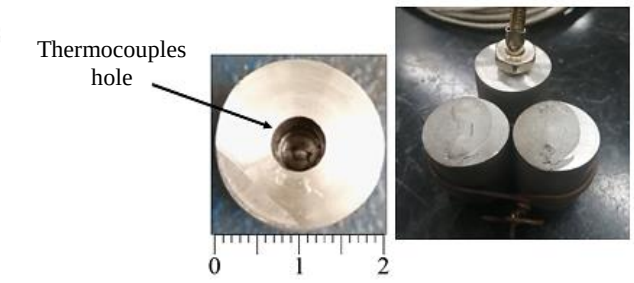

Figure 2 Workpieces for heat treatment inspection show a thermocouple hole. Scale in cm.

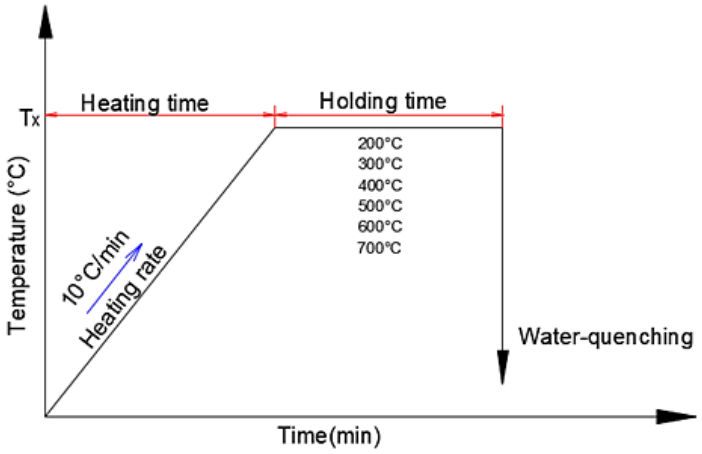

Figure 3 Temperature versus time for the temperature inspection/recrystallization state

2.3 Forging tests

Figure 4 illustrates a warm forging testing process. The workpieces were machined into cylinders with a diameter of 10 ±0.02 mm and a length of 20.70 mm. Forging used the die shape employed by Jhonthong and Talangkun [26]. Forging temperatures were 200, 300, 400, 500, 600, and 700 °C. Each specimen was held at its target temperature for approximately 5 minutes while the forging speed was 83.55 mm/s with a strain rate of 4 s^{-1}. After forging, all specimens were immediately cooled to room temperature using a water spray and then removed from the die.

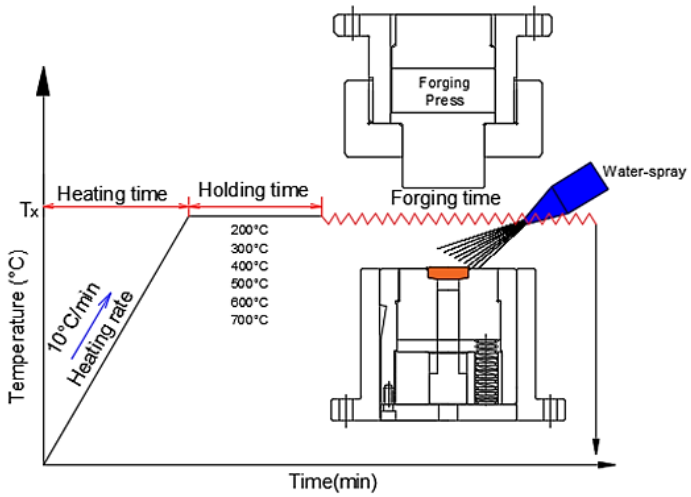

Figure 4 Temperature versus time for the deformation state during forging.

2.4 Microstructural examination

The microstructure of test specimens subjected to various heating temperatures was examined in the rolling direction. The surfaces were prepared by grinding (grit sizes 200-1200) followed by polishing. The specimen surfaces were etched with Nital (2% nitric acid, 98% ethanol). The microstructural examination was done using an optical microscope (Olympus BX60, Olympus Optical Co., Ltd., Tokyo, Japan). The percentage of pearlite and ferrite was measured by the point counting method. Additionally, a field-emission scanning electron microscope equipped for energy dispersive X-ray spectroscopy (EDS) (TESCAN Model MIRA, Tescan Orsay Holding, a.s., Brno-Kohoutovice, Czech Republic).

2.5 Hardness test

Initial specimen hardnesses were measured on a Rockwell hardness scale B using a Rockwell hardness testing machine (ERGOTEST DIGI 25 RS, GALILEO Durometria, Antegnate, Italy). Randomly selected specimens underwent testing at ten points. The points were 2 mm apart, as illustrated in Figure 5(a). Hardness values are presented as the average of two specimen measurements.

After-forging, specimen hardnesses were measured using a micro Vickers hardness test (HMV-G31S ENG 230V, SHIMADZU, Kyoto, Japan). Randomly selected specimens underwent testing in the vertical and horizontal directions in four of the deformation zones, as illustrated in Figure 5(b), including zone I (the hard deformation zone) zone II (the severe deformation zone) zone III (the free deformation zone) and zone IV (the sticking deformation zone). The hardness values are presented as the average of two specimen measurements.

(a) (b)

Figure 5 Hardness testing positions across the rolling direction of the specimens (a) Initial specimen, and (b) Forged specimen.

3. Results and discussion

3.1 Microstructure before forging

Figure 6(a) schematically shows the microstructure of the initial and test specimens produced by hot rolling and annealing. It was found that the microstructure of the AISI 1020 test specimen exhibited elongated ferrite grains along the rolling direction and pearlite phases in a banded structure also along the rolling direction, as shown in Figure 6(a). The grains still had a characteristic alternating ∝-carbide band structure, typical of the pearlite phase. When exposed to thermal energy, atom rearrangement occurred through a recovery mechanism, as depicted in Figures 6(b) at 200 °C to 6(e) at 500 °C. The ferrite phase maintained a similar structure to that at room temperature. However, at temperatures between 600 and 700 °C, dislocation movement and recrystallization of the ferrite grain boundaries increased. The stereological data of the microconstituents depicted in Table 2 is consistent with the theory that recrystallization of low-carbon steel occurs at approximately 0.4Tm (Tm: melting temperature) [27]. The original grains grew significantly and the pearlite phase diffused into pro-eutectoid ferrite, with Fe_3C transformed from a flat shape to a more rounded form, while still maintaining the rolling direction texture [24, 28], as shown in Figure 7.

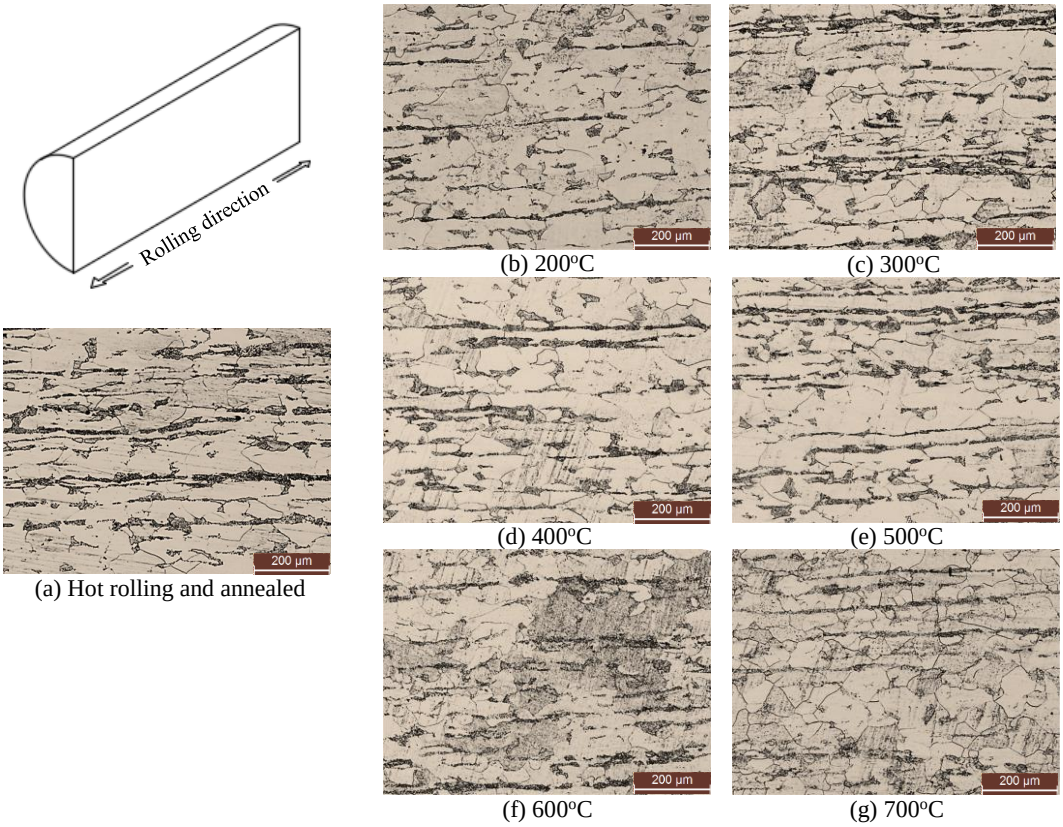

(a) Hot rolling and annealed (b) 200ºC (c) 300ºC (d) 400ºC (e) 500ºC (f) 600ºC (g) 700ºC

Figure 6 Initial microstructure and after heating to various temperatures.

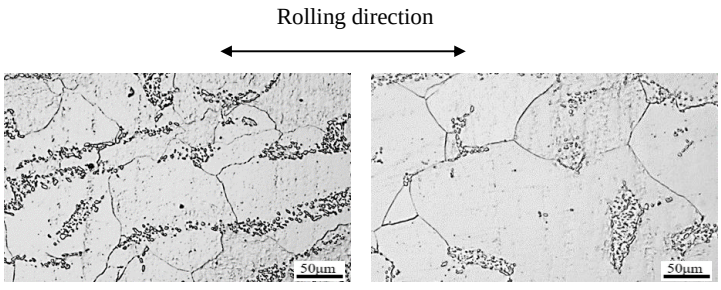

600ºC 700ºC

Figure 7 Micrographs of the characteristics of recrystallization and texture according to the rolling direction of 600 ºC and 700 ºC.

Table 2 Stereological data of the phases

Phase	Room Temp.	200 ºC	300 ºC	400 ºC	500 ºC	600 ºC	700 ºC
Ferrite (%)	80	76	69	67	62	59	57
Pearlite (%)	20	24	31	33	38	41	43

3.2 Microstructure after forging

Figure 8 shows the microstructure of the AISI 1020 test pieces after forging at different temperatures (200-700 °C). This analysis aids in the decision-making process for applying or referencing continuous warm forging processes in production design. The study considers the deformation behavior in 4 zones (I, II, III, IV) at 7 positions (P1-I to P7-IV) from the three test piece directions (compression direction (CD), transverse direction (TD), and normal direction (ND) [1, 29]. It was found that in Zone I at position P1-I and 200 °C (Figure 7(a)), the grains exhibited deformation and indicated flow of elongated grains along the TD plane due to compression. At 300-400 °C (Figures 7(b)-7(c)), the flow of elongated grains along the TD plane increased. However, as the temperature increased to 500-700 °C (Figures 7(d)-7(f)), newly recrystallized grains appeared, indicating a more pronounced occurrence of recrystallization. In Zone P1-I, grain formation from compressive forces became more evident, with prominent small round grains observed at 600-700 °C (Figures 7(e)-7(f)). In Zone I at position P3-I, the grains remained aligned in the initial rolling direction due to the lower applied deformation forces. At 300-400 °C, the grains in this region deformed more effectively due to the higher temperature, resulting in increased grain flow along the TD plane. Newly recrystallized grains, larger than those in Zone P1-I, became more prominent as the temperature increased to 600-700 °C. In Zone II, at 200-700 °C, the most severe deformation occurred due to the action of triaxial compressive stress. Newly recrystallized grains began to appear at 500 °C and became more prominent at 600–700 °C. In Zone III at positions P4-III and P6-III, the material flow was influenced by bidirectional forces, i.e., compressive force in the CD and tensile force in the transverse direction (TD). This is referred to as "the free deformation zone" [25, 30]. At 200-400 °C, deformed grain structures were visible, increasing with higher temperatures (500-700 °C) along the radial direction of the workpiece, controlled by the die boundaries. The microstructure of Zone IV at 200–400 °C, as shown in areas P5–IV and P7–IV, exhibited increasingly irregular grain shapes due to compression against the die walls in all three directions. As the temperature increased, newly recrystallized grains appeared at 500–600 °C and became more distinct at 700 °C. In these experiments, no internal cracks were observed because the initial workpiece underwent annealing and was forged at temperatures higher than room temperature with low effective stress. This finding is consistent with the research of Jhonthong and Talangkun [26] and Dalbosco et al. [30].

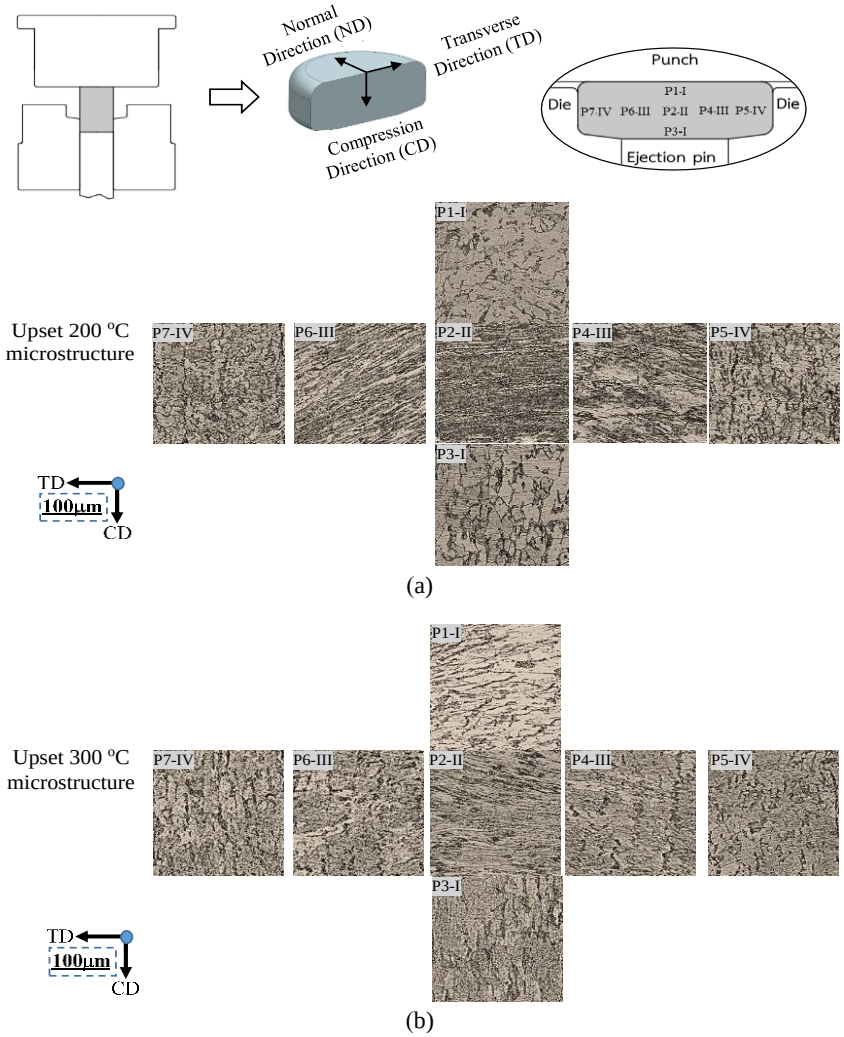

Figure 8 Transverse microstructure of warm forged specimens from various areas. Upset at (a) 200 ºC, (b) 300 ºC, (c) 400 ºC, (d) 500 ºC, (e) 600 ºC, and (f) 700 ºC.

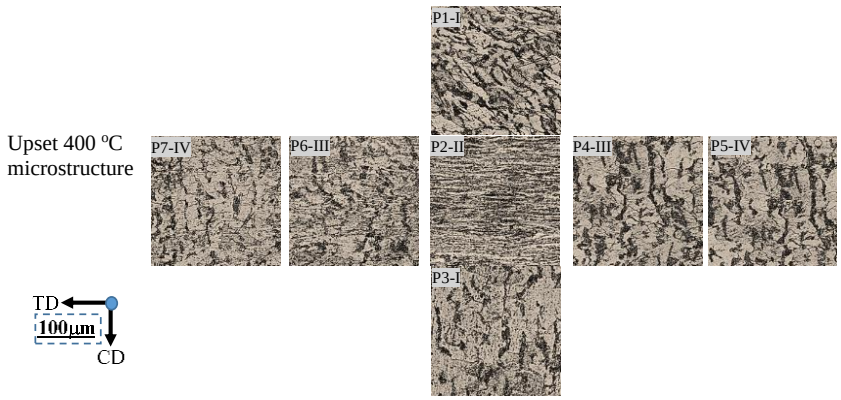

(c)

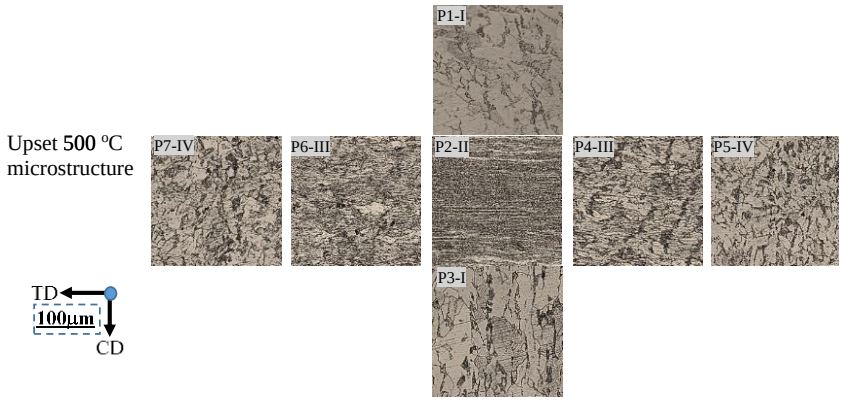

(d)

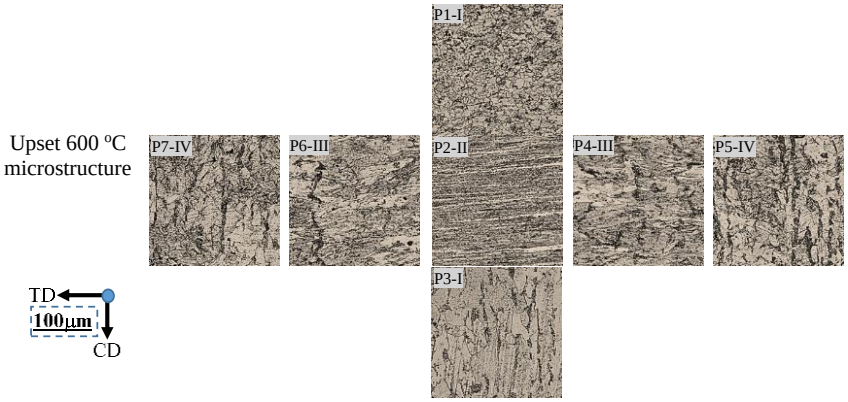

(e)

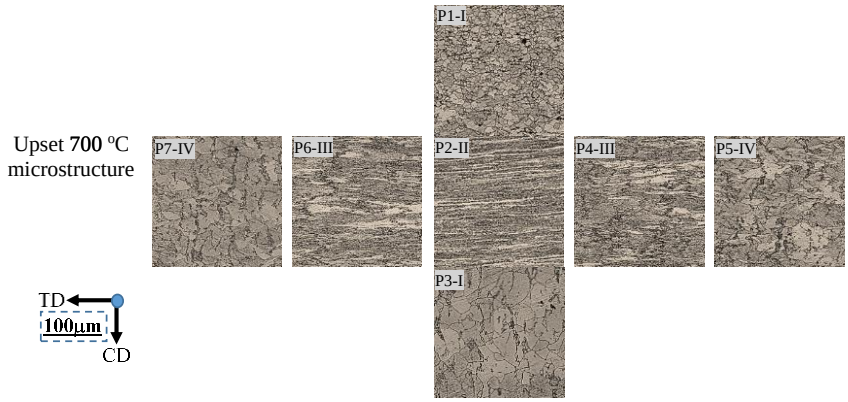

(f)

Figure 8 (continued) Transverse microstructure of warm forged specimens from various areas. Upset at (a) 200 ºC, (b) 300 ºC, (c) 400 ºC, (d) 500 ºC, (e) 600 ºC, and (f) 700 ºC.

Figure 9 shows high magnification of the microstructure in Zone II to study the 3-dimensional structure subjected to forging process forces at temperatures ranging from 200 to 700 °C, compared to the structure forged at room temperature, as done by Jhonthong and Talangkun [26] The results of this experiment can be divided into three levels. At the first level, at a temperature of 200 °C, the grain structure still resembles that of a room-temperature forged specimen, with elongated grains aligned with the compression force. Fe_3C in pearlite exhibited globule carbide instead of a laminar form as found in pearlite. As the temperature was increased to 300–400 °C, carbides broke up and were dispersed due to the flow induced by the applied compression force. When forged at 500 °C, pro-eutectoid ferrite deformed recrystallized ferrite grains at the eutectoid ferrite phase, which was previously pearlite. When subjected to higher thermal energy and semi-closed die compression at 600 °C, new eutectoid ferrite phases recrystallized, and carbide was distributed throughout the structure. At 700 °C, the recrystallized grains grew.

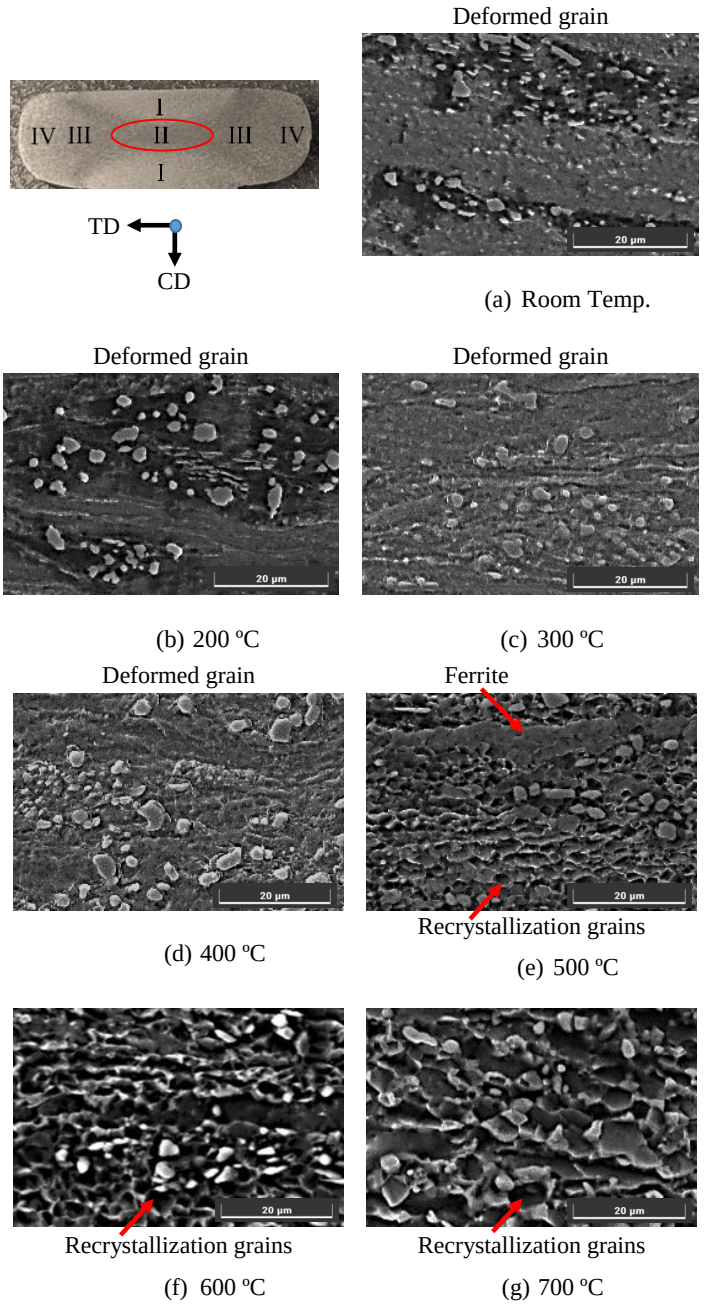

Figure 9 SEM images showing microstructure after warm forging at various temperatures.

3.3 Hardness of the forged specimen

Figure 10 shows the average hardness of the forged specimens at temperatures ranging from 200-700 °C, following the procedures outlined in section 2.3 under Experimental Setup and Procedures/Methods. Hardness values are critical in determining the appropriate temperature for warm forging. From experimental findings in the x-axis "large deformation zone" (Zone P2-II) at 700 °C, the lowest average hardness was 236 HV. In contrast, in contact with the punch and die, Zone I, known as "the hard deformation zone", position P1-I exhibited higher hardness than P3-I due to increased surface contact and concurrent strain hardening. At 700 °C, the lowest average hardness was 228 HV at position P1-I and 174 HV at position P3-I. At 200 °C, as shown in Figure 10(a), Zone II (P2-II) remains a large deformation zone, while Zone III is "the free deformation zone" (P4-III, P6-III) with the lowest average hardness, 213 HV. On the y-axis, Zone IV (P5-IV, P7-IV), subjected to die wall compression, remains in a tri-axial strain-hardened state with an

average hardness ranging from 220–227 HV at 600–700 °C, as shown in Figure 10(b). The findings of three to four deformation zones are consistent with the studies of Jhonthong and Talangkun [26] and Lei et al. [29]. Furthermore, higher hardness is attributed to increased effective strain in Zone II [1-3, 31]. In addition, during the forging process, the material is compressed, resulting in microstructural changes, which cause the accumulation of stress energy within the material. The increased density of dislocation hinders the movement of crystal planes within the material, the interaction of dislocations resulting in increased strength and hardness of the material.

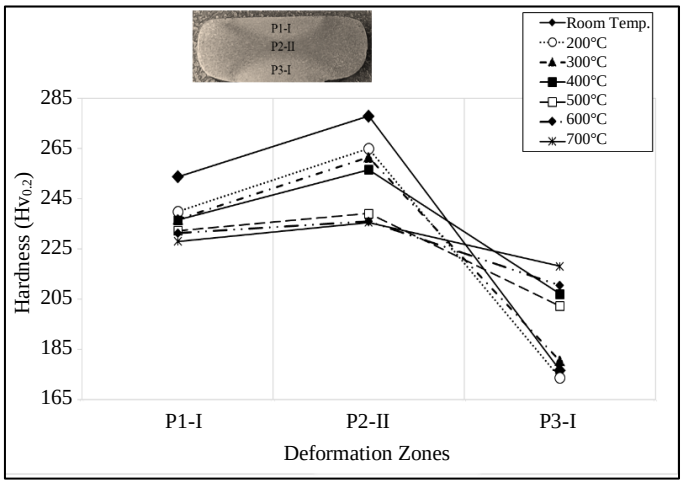

(a) Average hardness of forged specimens on the x-axis.

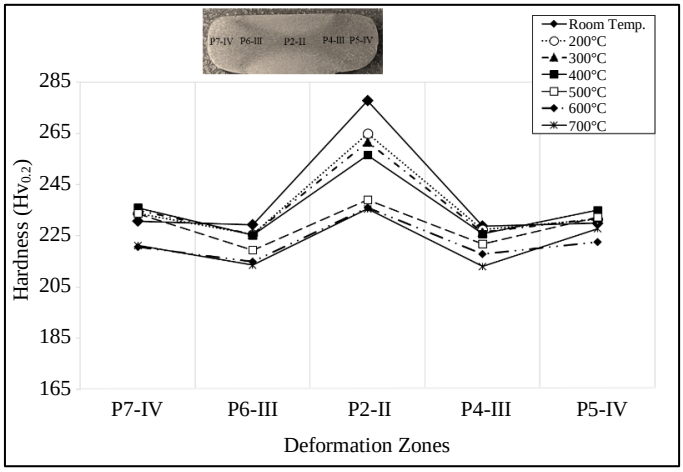

(b) Average hardness of forged specimens on the y-axis.

Figure 10 Average hardness of the forged specimens on the x-y axis.

3.4 Benefits of a warm forged specimen microstructure

The current research studied the effect of warm deformation parameters on the hardness and microstructure of AISI 1020 low-carbon steel to minimize the number of steps in a multi-step cold forging manufacturing process. This material is widely used in automotive parts manufacture. The proposed process reduces the number of production steps and required processing time. It also improves the mechanical properties of parts after the forging process. Figure 11 shows a comparison of the current process for cold forging and warm forging. In a warm forging process, slugs are heated to a temperature below the recrystallization temperature. After that, forging is continuously done until the final step with no reheating or process annealing. Throughout the forging process, graphite lubricant is sprayed to lubricate the workpiece and the die, preventing sticking. This also extends the die life. From this research on warm forging of AISI 1020 low-carbon steel, the microstructure began to recrystallize at 500 °C and became more pronounced at 600–700 °C. The hardness value in the upset stage had a minimum average hardness of 174 HV and a maximum average of 265 HV after water cooling. Compared with current cold forging processes, the average hardness was 171 HV in the upset stage. In cold forging Step 1, the maximum average hardness was 189 HV. However, in cold forging Step 2, without annealing after forging, the maximum average measured hardness was 251 HV. The hardness of the workpiece before warm forging was approximately 29 percent higher than in cold forging processes. However, in the warm forging process, the workpiece remains warm throughout all stages of forging. Thus, the hardness of the in-process workpiece would be lower than measured when the workpiece has been cooled. Additionally, one of the advantages of warm forging is that it reduces the number of production steps from 9 in the current process to just 3. Furthermore, these 3 steps are part of a continuous production process, eliminating the waiting time needed for softening adjustments before subsequent forging steps.

Production processes become more efficient with machinery operating with sequential sub-processes (Figures 12(a–b)) equipped with devices for adjusting material temperature before forging and a graphite lubricant spraying system. Figure 12(b) shows the characteristics of a warm slug in a multi-station machine press forging process, which leads to reduced machine energy consumption and lower production costs, as discussed by Lee et al. [32].

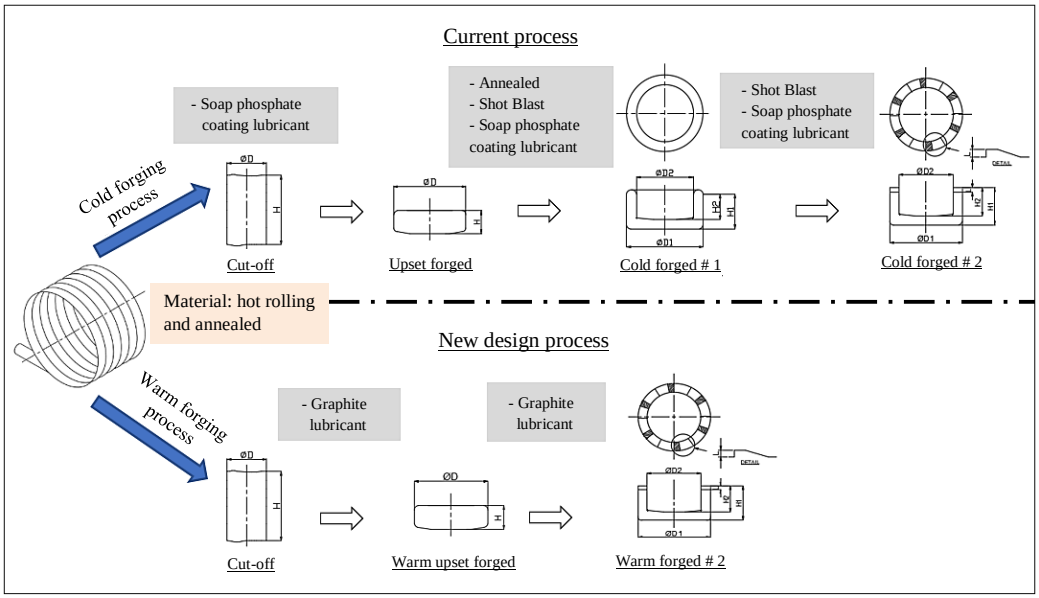

Figure 11 Comparison of the current (cold forging) and new (warm forging) processes.

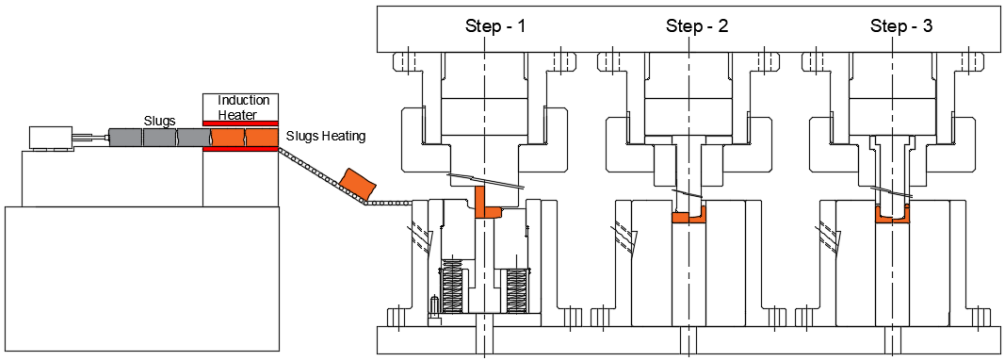

(a) Characteristics of a warm slug in a step-by-step machine press forging process.

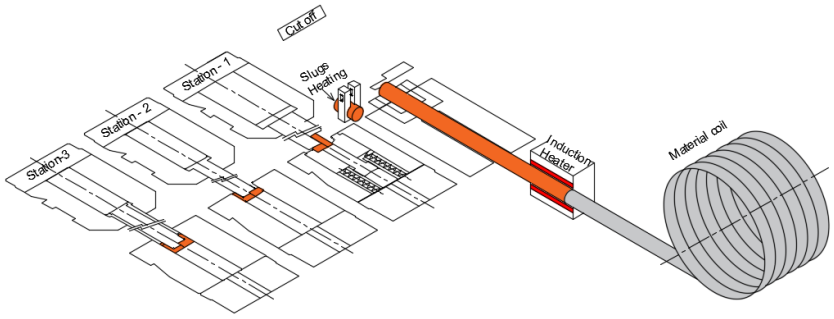

(b) Characteristics of a warm slug in a multi-station machine press forging process.

Figure 12 Characteristics of warm slugs using mechanical continuous forging.

4. Conclusions

From the experimental results, the following conclusions can be drawn:

1. Before forging, it has been observed the string of pearlite along the roll direction with grain growth. When thermally stimulated, the recovery mechanism rearranges atoms slightly. From 200 to 500 °C, there is an increase in grain growth. As more thermal energy is added, the ferrite structure's grain boundaries re-crystallize and grow, as seen in the 600 to 700 °C temperature range. Meanwhile, pearlite decomposes into carbide and retains its rolling direction.

2. After forging at 700 °C, the lowest average hardness, 236 HV, was found along the x-axis in the "large deformation zone" (Zone P2-II). In the "hard deformation zone" (Zone I), especially at position P1-I, hardness was higher due to three-dimensional compressive stress. The lowest average hardness was 174 HV at 200 °C. It was 228 HV at 700 °C and position P1-I.

3. After forging, along the y-axis, Zone II (P2-II) remains the largest deformation zone. However, Zone III becomes the “free deformation zone” (P4-III, P6-III), with the lowest average hardness, 213 HV at 200 °C. In Zone IV (P5-IV, P7-IV), specimens compressed against the die wall experience triaxial compressive stress, with an average hardness of 220–227 HV at 600–700 °C. The observed microstructure shows deformed grains indicating grain flow, with elongated grains along the TD plane at 200–400 °C. Newly recrystallized grains appear at 500 °C. As the temperature increases to 600–700 °C, more prominent grain growth is observed.

4. Considering the application of warm forging processes, the most suitable temperature range for AISI 1020 is below 500 °C, as the primary microstructure in the forging process has not yet undergone recrystallization.

5. Acknowledgements

The authors express their deepest appreciation to Rajamangala University of Technology Isan, Sakon Nakhon Campus, Research and Graduate Studies, Supply Chain and Logistics System Research Unit, and Faculty of Engineering, Khon Kaen University for playing a decisive role in facilitating and providing all the precious research tools and funding.

6. References

[1] Tschaetsch H. Metal forming practise: processes, machines, tools. Berlin: Springer; 2006.
[2] Altan T, Ngaile G, Shen G. Cold and hot forging: fundamentals and applications. Ohio: ASM international; 2004.
[3] AIDA Engineering. AIDA press handbook. 4th ed. Japan: AIDA Engineering Ltd; 2007.
[4] Hirscvogel M, Dommelen HV. Some applications of cold and warm forging. J Mater Process Technol. 1992;35(3-4):343-56.
[5] Islam T, Rashed HMMA. Classification and application of plain carbon steels. Reference module in materials science and materials engineering. Amsterdam: Elsevier. 2019.
[6] Reddy PPK, Dewangan S, Singh RS, Singhal U, Biswas A. Heat treatment effects on microstructure and hardness of low-carbon AISI 1020 steel. J Inst Eng India: Ser D. 2024:1-12.
[7] Sun J, Li J, Wang P, Huang Z. Hot deformation behavior, dynamic recrystallization and processing map of Fe–30Mn–10Al–1C low-density steel. Trans Indian Inst Met. 2022;75:699-716.
[8] Qiu P, Han Y, Huang G, Le J, Lei L, Xiao L, et al. Texture evolution and dynamic recrystallization behavior of hybrid-reinforced titanium matrix composites: enhanced strength and ductility. Metall Mater Trans A. 2020;51(5):2276-90.
[9] Dehghan-Manshadi A, Barnett MR, Hodgson PD. Microstructural evolution during hot deformation of duplex stainless steel. Mater Sci Technol. 2007;23(12):1478-84.
[10] Zhao Q, Li F, Zhu E, Gopi KR, Farah S, An X, et al. Investigation on the grain structure evolution and abnormal stress increase of Al–Mg–Si alloy during hot deformation. Met Mater Int. 2024;30(4):967-89.
[11] Su G, Liu Y, Xiao X, Du J, Zhang P, Shen X. Influences of stress state, temperature, and strain rate on ductility of pure iron. J Mater Eng Perform. 2021;30:2036-46.
[12] Chamanfar A, Chentouf SM, Jahazi M, Lapierre-Boire LP. Austenite grain growth and hot deformation behavior in a medium carbon low alloy steel. J Mater Res Technol. 2020;9(6):12102-14.
[13] Hamada AS, Somani MC, Karjalainen LP. High temperature flow stress and recrystallization behavior of high-Mn TWIP steels. ISIJ Int. 2007;47(6):907-12.
[14] Edalati K, Wang Q, Enikeev NA, Peters LJ, Zehetbauer MJ, Schafler E. Significance of strain rate in severe plastic deformation on steady-state microstructure and strength. Mater Sci Eng A. 2022;859:144231.
[15] Ferro P, Bonollo F, Bassan, F, Berto F. Strain evolution in cold-warm forged steel components studied by means of EBSD technique. Materials. 2017;10(12):1441.
[16] Zhao F, Hu H, Liu X, Zhang Z, Xie J. Effect of billet microstructure and deformation on austenite grain growth in forging heating of a medium-carbon microalloyed steel. J Alloys Compd. 2021;869:159326.
[17] Nasiri Z, Ghaemifar S, Naghizadeh M, Mirzadeh H. Thermal mechanisms of grain refinement in steels: a review. Met Mater Int. 2021;27:2078-94.
[18] Dolzhenko A, Tikhonova M, Kaibyshev R, Belyakov A. Microstructures and mechanical properties of steels and alloys subjected to large-strain cold-to-warm deformation. Metals. 2022;12(3):454.
[19] Kim KM, Kang CG. Forgebility evaluation of SNCM 220 steel by warm compression test and microstructure behaviors characteristics. Int J Precis Eng Manuf-Green Technol. 2016;3:105-10.
[20] Huang W, Lei L, Fang G. Microstructure evolution of hot work tool steel 5CrNiMoV throughout heating, deformation and quenching. Mater Charact. 2020;163:110307.
[21] Yan X, Zhang S, Huang K, Yang Y, Wang W, Wu M. Effect of holding time on the extrusion force and microstructure evolution during the plastic forming of Ti-6Al-4V micro-gears. Materials. 2020;15(4):1507.
[22] Wang H, Cao L, Li Y, Schneider M, Detemple E, Eggeler G. Effect of cooling rate on the microstructure and mechanical properties of a low-carbon low-alloyed steel. J Mater Sci. 2021;56:11098-113.
[23] Sugimoto KI, Hojo T, Srivastava AK. Low and medium carbon advanced high-strength forging steels for automotive applications. Metals. 2019;9(12):1263.
[24] Çalik A. Effect of cooling rate on hardness and microstructure of AISI 1020, AISI 1040 and AISI 1060 Steels. Int J Phys Sci. 2009;4(9):514-8.
[25] Abbaschian R, Abbaschian L, Reed-Hill RE. Physical metallurgy principles. 4th ed. Stamford: Cengage Learning; 2009.
[26] Jhonthong N, Talangkun S. Design of the semi-closed die for shaping the thick coin-like carbon steel parts in a single operation. SN Appl Sci. 2023;5(7):176.
[27] Callister WD, Rethwisch DG. Materials science and engineering: an introduction. 10th ed. Hoboken: Wiley; 2018.
[28] Wang S, Chen M, Yang M, Huang Y, Wang S, Mao X. Effect of cold rolling reduction rate on the microstructure and properties of Q&P steel with a ferrite-pearlite initial structure. Materials. 2023;16(18): 6102.
[29] Lei J, Ma L, Jia W, Le Q, Pan H, Yuan Y. Zonal differences in deformation characteristics of AZ31 Mg alloy constrained by heterogeneous metals. J Mater Res Technol. 2021;13:2161-79.
[30] Dalbosco M, da Silva Lopes G, Schmitt PD, Pinotti L, Boing D. Improving fatigue life of cold forging dies by finite element analysis: a case study. J Manuf Process. 2021;64:349-55.
[31] Narayanan RG, Gopal M, Rajadurai A. Infuence of friction in simple upsetting and prediction of hardness distribution in a cold forged product. J Test Eval. 2008;36(4):371-83.
[32] Lee Y, Yoon E, Nho T, Moon Y. Microstructure control of ferrous driven part fabricated by warm precision forging. Procedia Manuf. 2018;15:404-10.